

Probing the Effect of Nitro-substituents in the Modulation of LUMO Energies for Directional Electron Transport through 4d⁶ Ruthenium(II)-based Metallosurfactants

Samudra Amunugama,^a Eyrarn Asempa,^b Elena Jakubikova,^{*,b} Cláudio N. Verani^{*,a}

(a) Department of Chemistry, Wayne State University, Detroit, MI 48202, USA.

(b) Department of Chemistry, North Carolina State University, Raleigh, NC 27695, USA

Outline

Figure S1. ESI mass spectrum of complex **1-3 (a-c)**

Figure S2. ¹H-NMR spectrum of 4'-(4-(octadecyloxy)phenyl)-2,2':6'2''-terpyridine (L^{terpy}) ligand

Figure S3. ¹H-NMR spectrum of 4'-(4-nitrophenyl)-2,2':6',2''-terpyridine (tpy^{NO2})

Figure S4. COSY NMR spectrum of complex [Ru(tpy^{OC18})(tpy)](PF₆)₂ **1**

Figure S5. HSQC NMR spectrum of complex [Ru(tpy^{OC18})(tpy)](PF₆)₂ **1**

Figure S6. COSY NMR spectrum of complex [Ru(tpy^{OC18})(phen)Cl](PF₆) **3**

Figure S7. HSQC NMR spectrum of complex [Ru(tpy^{OC18})(phen)Cl](PF₆) **3**

Figure S8. HSQC NMR spectrum of complex [Ru(tpy^{OC18})(phen^{NO2})Cl](PF₆) **4**

Figure S9. UV-visible spectrum of complexes **1-4** in 1 x 10⁻⁵ M dichloromethane solution

Table T1. UV-visible data for complexes **1-4**

Table T2. Redox potentials vs Fc/Fc⁺ for complexes **1-4**

Figure S10. Isothermal compression data of complexes **1-4 (a-d)**

Figure S11. BAM Images of Complexes **1, 2** and **3**

Table T3. Transfer ratios of monolayers of complexes **1-4**

Figure S12. Comparison of UV-vis spectrum of LB films and solution state UV-vis spectrum of **3**

Figure S13. Comparison of UV-vis spectrum of LB films and solution state UV-vis spectrum of **4**

Figure S14. Comparison between IR spectrum of complex **4** in KBr and IRRAS spectrum of 47-layer LB film.

Figure S15. Comparison between IR spectrum of complex **3** in KBr and IRRAS spectrum of 47-layer LB film.

Figure S16. Mass spectrum of [Ru(tpy^{OC18})(phen)Cl](PF₆) **3** recovered from LB films

Figure S17. Mass spectrum of [Ru(tpy^{OC18})(phen^{NO2})Cl](PF₆) **4** recovered from LB films

Figure S18. AFM images of complex **4** deposited at 17, 20, 24, and 28 mN/m

Table T4. Summary of surface roughness data of LB monolayers of complex **3** and **4** deposited at different pressures

Figure S19. Asymmetric ruthenium(II) complexes investigated in the theoretical section (the -C₁₈H₃₇ group was replaced by a -CH₃ group)

Figure S20. (a) Fragment orbital analysis of the singlet state of **1-3 (a-c)** in dichloromethane

Figure S21. Ground state (singlet) frontier molecular orbitals of **1-3** complexes

Figure S22. Molecular orbital diagram of asymmetric Ru complexes in their singlet ground state. MO colors correspond to their character; blue - metal-based, green - MeO-terpyridine-based,

purple - mixed character with contributions from Ru metal and MeO-terpyridine, brown - substituted terpyridine based, black – mixed character with contributions from MeO-terpyridine and substituted terpyridine, red - phenanthroline based)

Figure S23. Natural orbitals (for open shell species) and molecular orbitals (for closed shell species) of the oxidized and reduced species of an asymmetric Ru complex **1** in dichloromethane. Orbital occupancy is shown for each orbital (0.0 – unoccupied orbital, 1.0 – singly-occupied orbital, 2.0 – doubly-occupied orbital)

Figure S24. Natural orbitals (for open shell species) and molecular orbitals (for closed shell species) of the oxidized and reduced species of an asymmetric Ru complex **2** in dichloromethane. Orbital occupancy is shown for each orbital (0.0 – unoccupied orbital, 1.0 – singly-occupied orbital, 2.0 – doubly-occupied orbital)

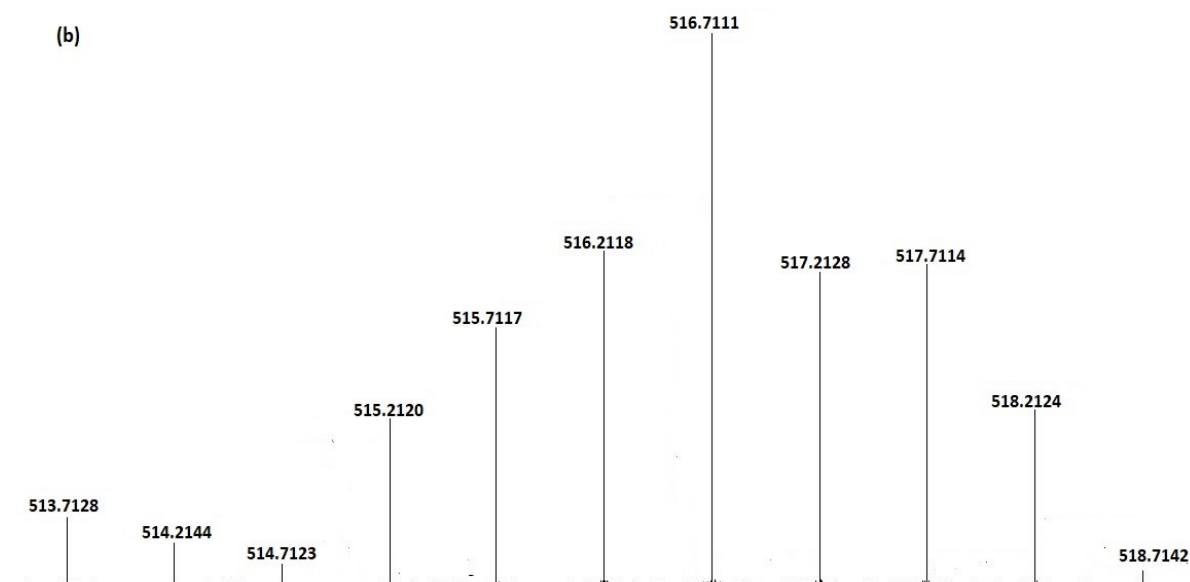
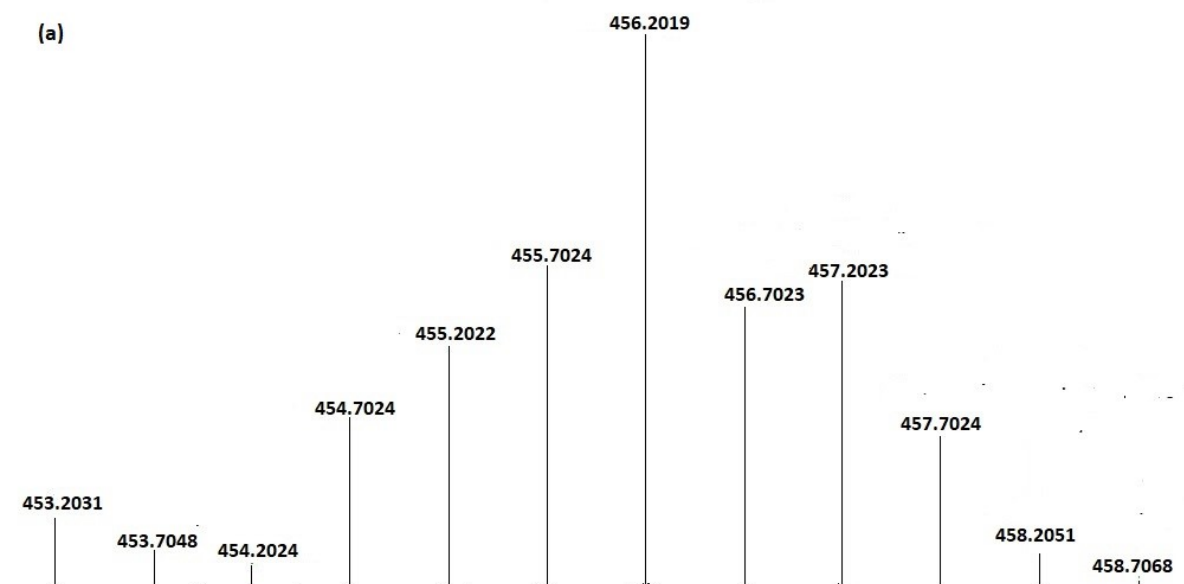
Figure S25. Natural orbitals (for open shell species) and molecular orbitals (for closed shell species) of the oxidized and reduced species of an asymmetric Ru complex **3** in dichloromethane. Orbital occupancy is shown for each orbital (0.0 – unoccupied orbital, 1.0 – singly-occupied orbital, 2.0 – doubly-occupied orbital)

Figure S26. Natural orbitals (for open shell species) and molecular orbitals (for closed shell species) of the oxidized and reduced species of an asymmetric Ru complex **4** in dichloromethane. Orbital occupancy is shown for each orbital (0.0 – unoccupied orbital, 1.0 – singly-occupied orbital, 2.0 – doubly-occupied orbital)

Table T5: Electrochemical data for asymmetric Ru(II) complexes in dichloromethane (PCM solvent model), S = singlet, D = doublet and T = triplet

Figure S27. I-V characteristics of complex **4** in four devices

Figure S1: ESI mass spectrum of complex 1-3 (a-c)



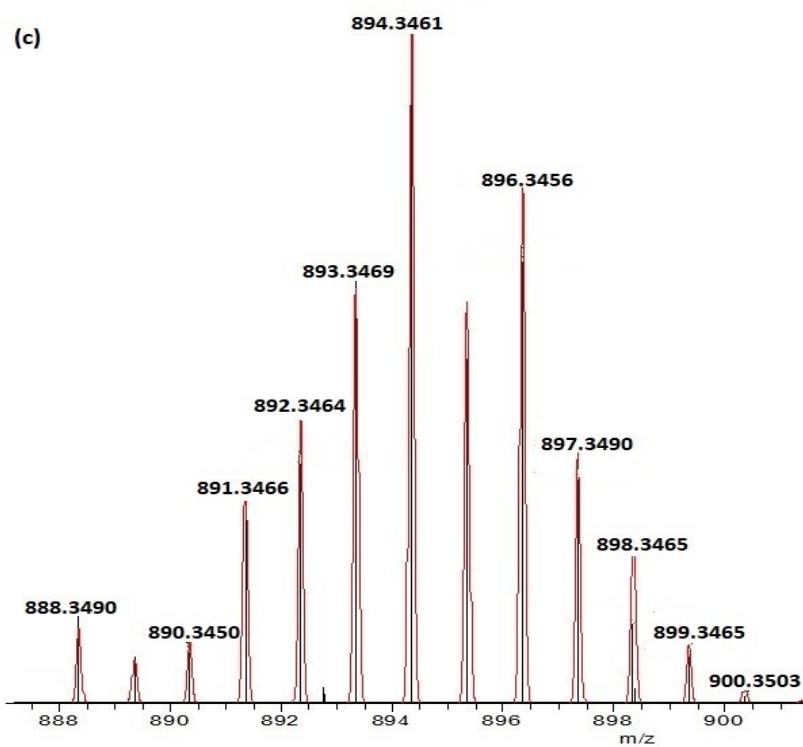


Figure S2: $^1\text{H-NMR}$ spectrum of 4'-(4-(octadecyloxy)phenyl)-2,2':6'2''-terpyridine (L^{terpy}) ligand

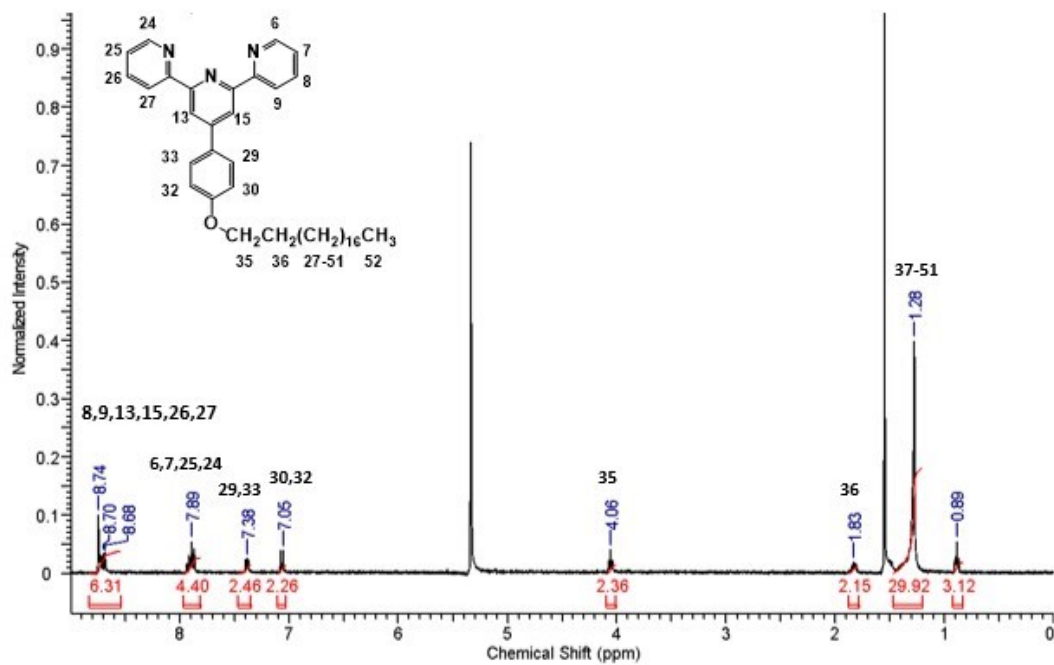


Figure S3: $^1\text{H-NMR}$ spectrum of 4'-(4-nitrophenyl)-2,2':6',2''-terpyridine (tpy^{NO_2})

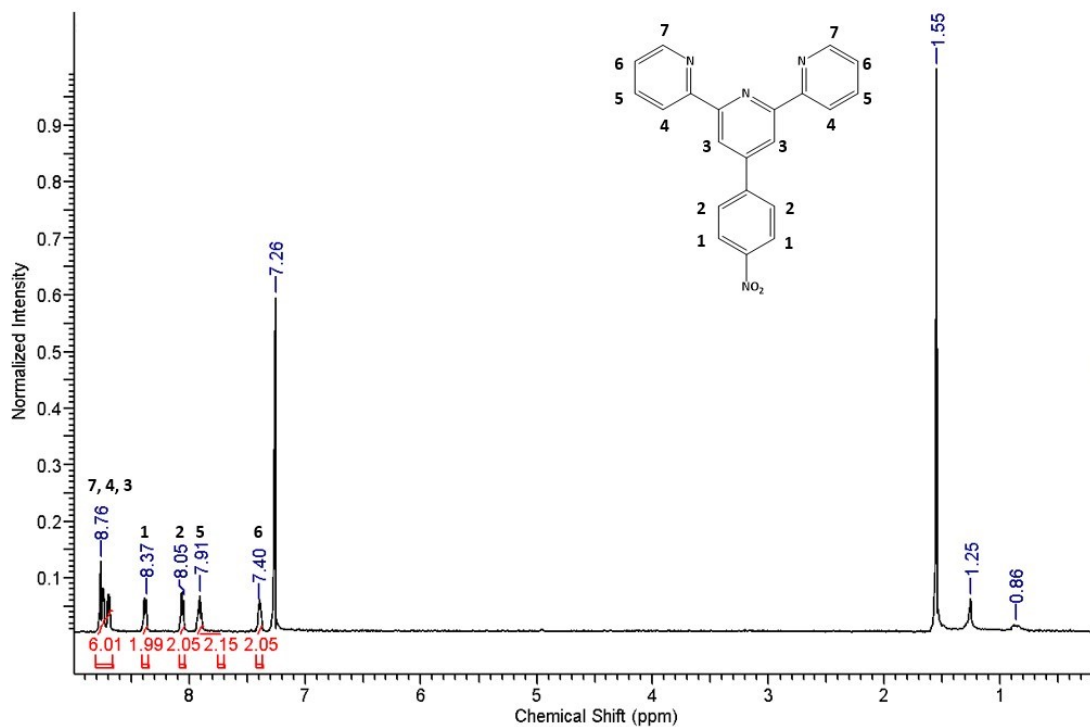


Figure S4: COSY NMR spectrum of complex $[\text{Ru}(\text{tpy}^{\text{OC18}})(\text{tpy})](\text{PF}_6)_2$ **1**

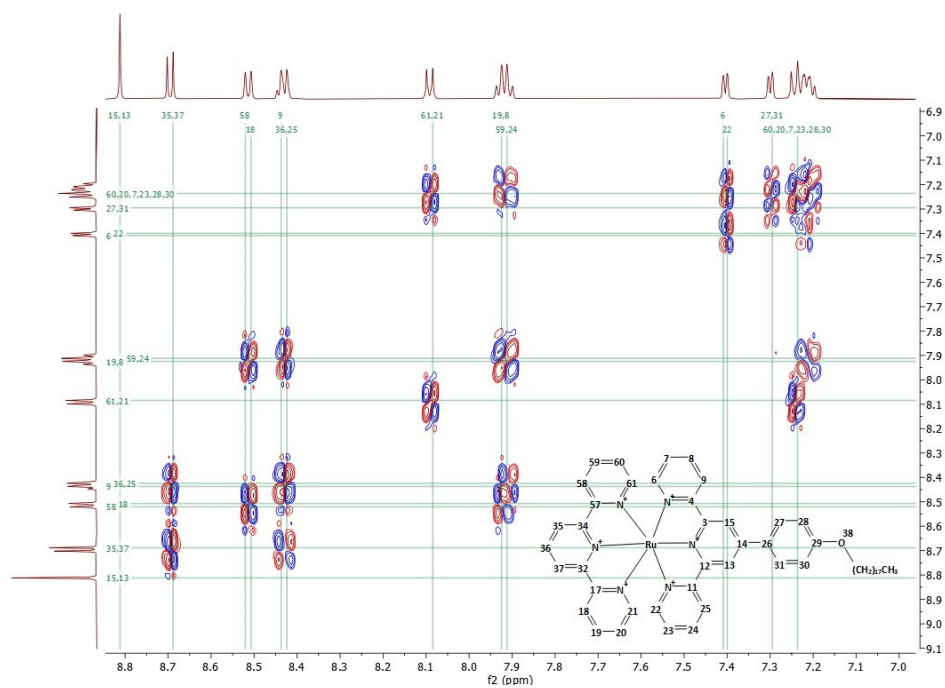


Figure S5: HSQC NMR spectrum of complex $[\text{Ru}(\text{tpy}^{\text{OC18}})(\text{tpy})](\text{PF}_6)_2$ **1**

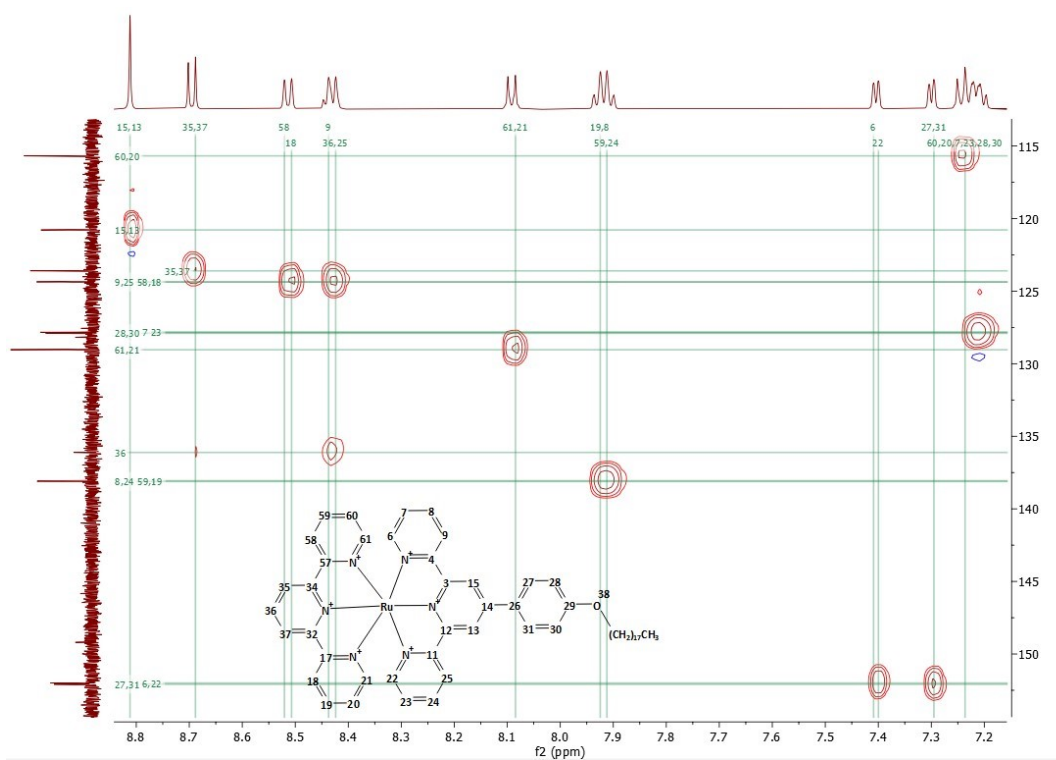


Figure S6: COSY NMR spectrum of complex $[\text{Ru}(\text{tpy}^{\text{OC18}})(\text{phen})\text{Cl}](\text{PF}_6)$ **3**

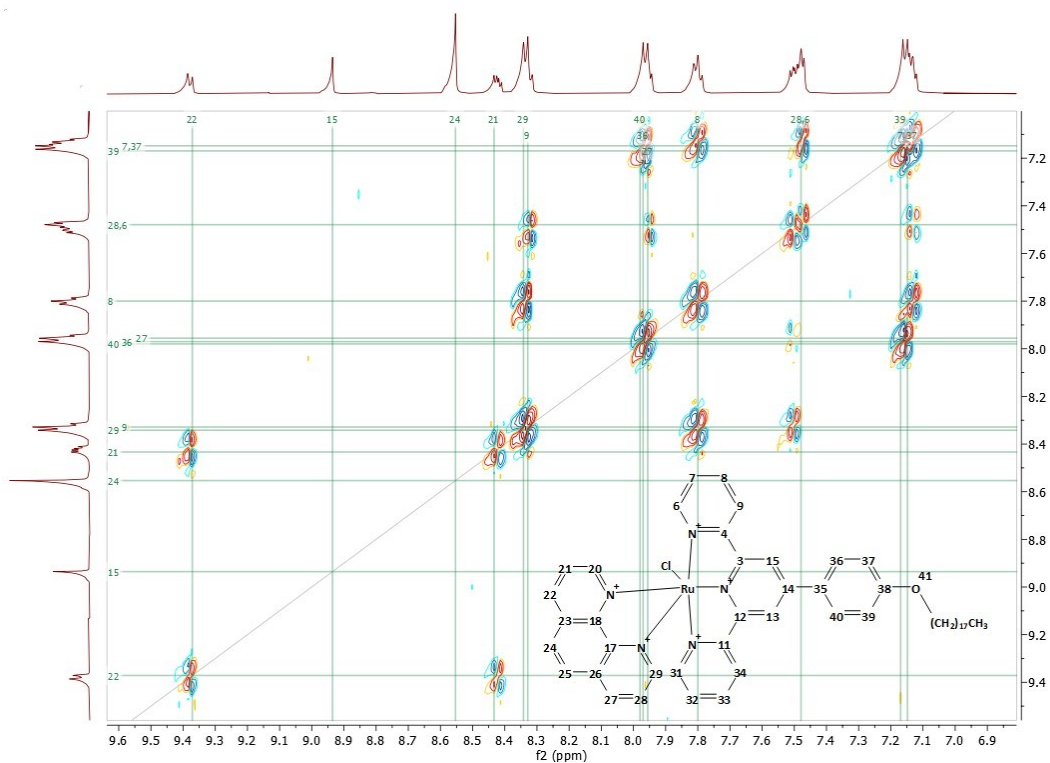


Figure S7: HSQC NMR spectrum of complex [Ru(tpy^{OC18})(phen)Cl](PF₆) 3

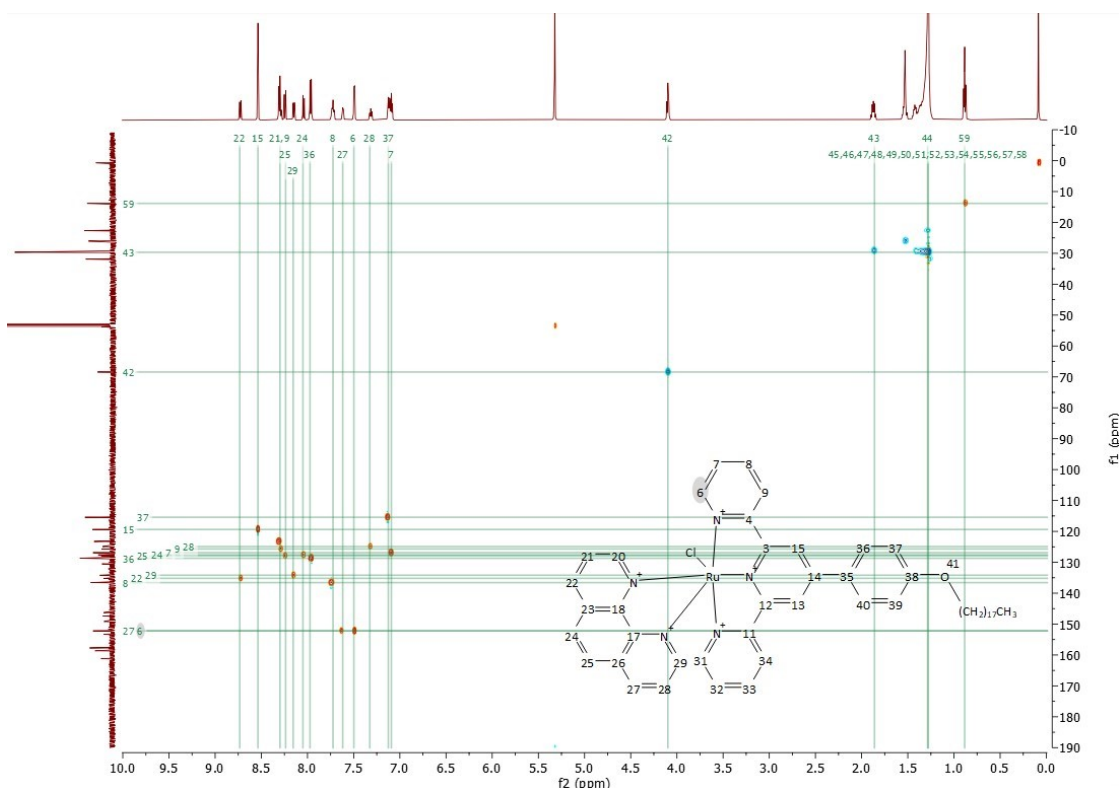


Figure S8: HSQC NMR spectrum of complex [Ru(tpy^{OC18})(phen^{NO2})Cl](PF₆) 4

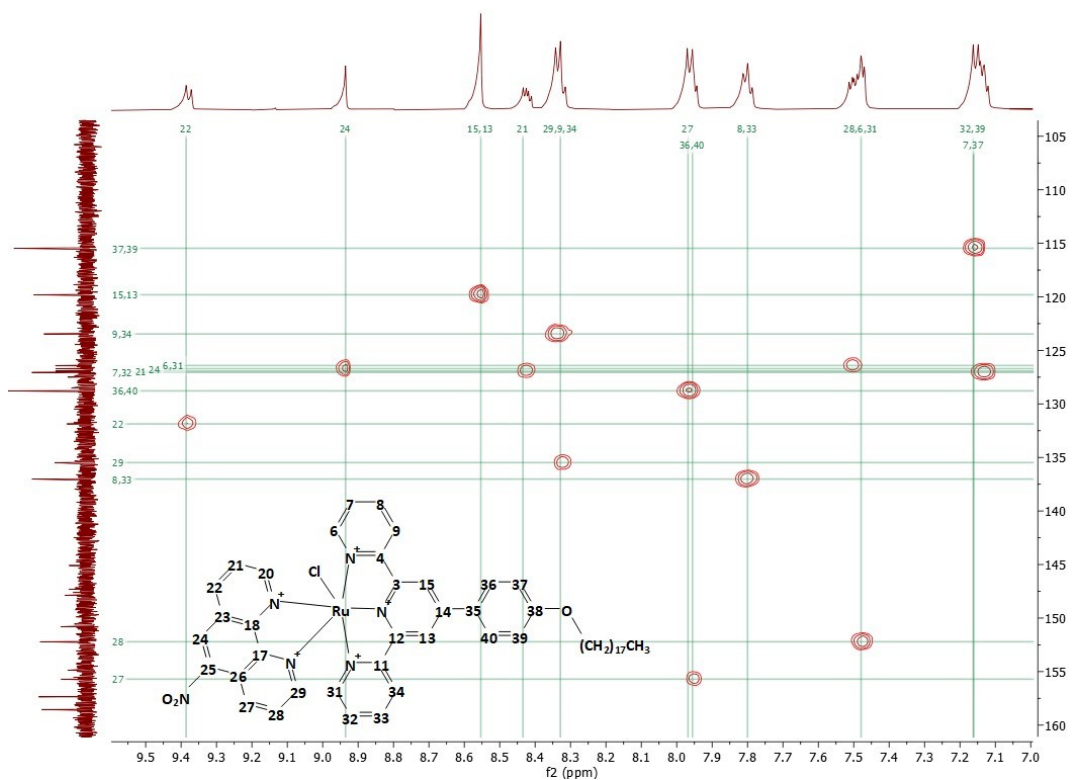


Figure S9: UV-visible spectrum of complexes **1-4** in 1×10^{-5} M dichloromethane solution

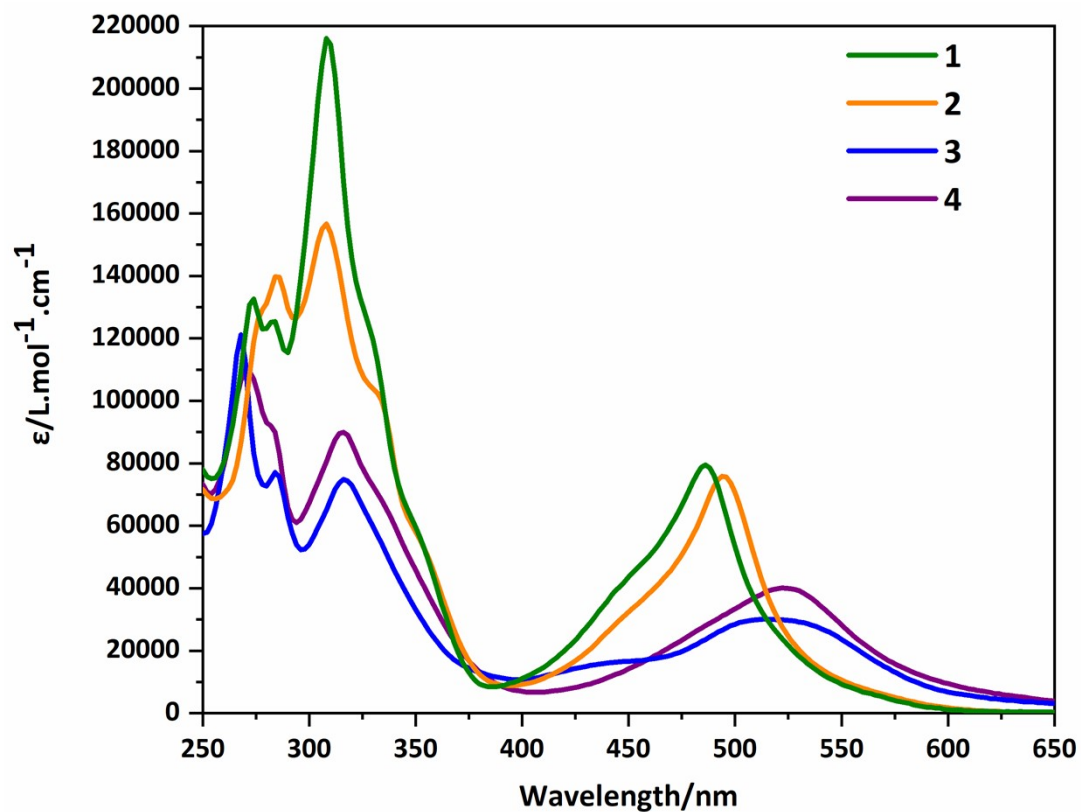


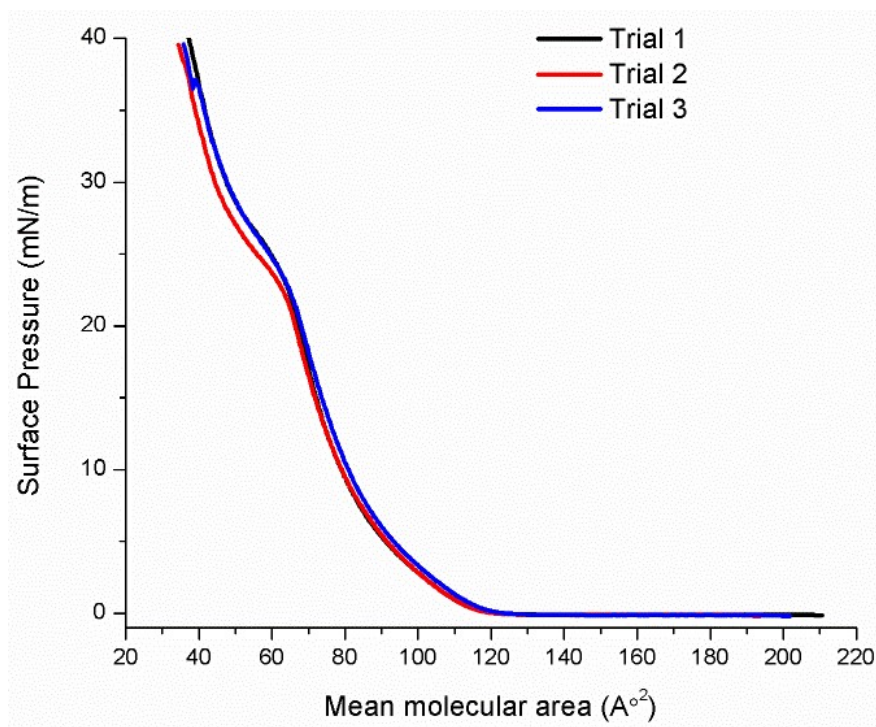
Table T1: UV-visible data for complexes **1-4**

Complex	λ_{max} , nm (ϵ , $\text{L}\cdot\text{mol}^{-1}\cdot\text{cm}^{-1}$) CH_2Cl_2
1	232, 274, 308, 486
2	236, 284, 308, 494
3	232, 268, 316, 514
4	240, 272, 316, 522

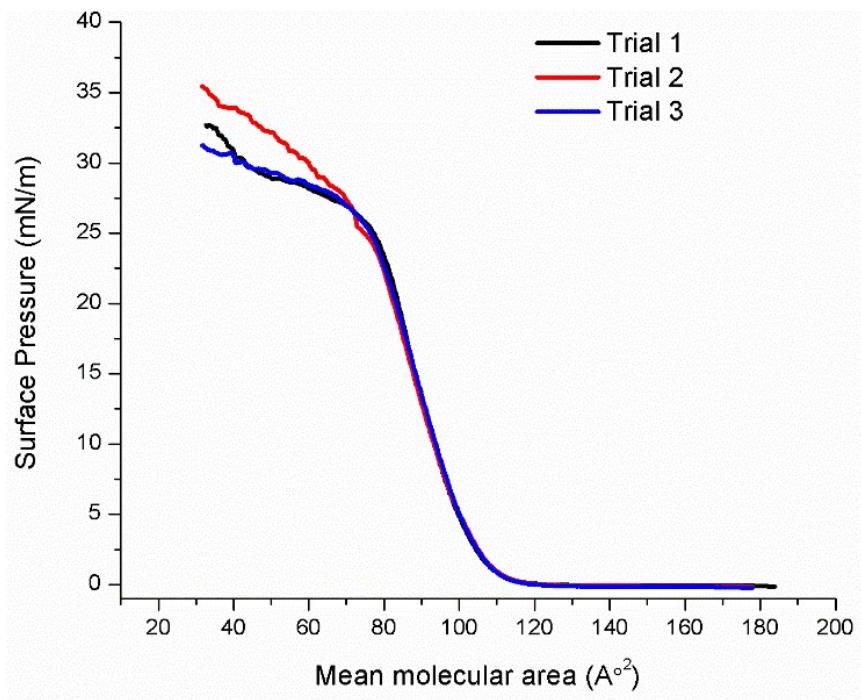
Table T2: Redox potentials vs Fc/Fc⁺ for complexes 1-4

Process vs Fc/Fc ⁺ Compound	E _{1/2} (ΔE _p)/V			
	I _{pa} /I _{pc}			
1	869 0.72	-1675 1.16	-1987 1.32	
2	879 0.60	-1383 1.73	-1563 0.82	-1941
3	346 0.70	-1919 2.74	-2370	
4	479 0.79	-1058 1.44	-1704 2.71	-1958

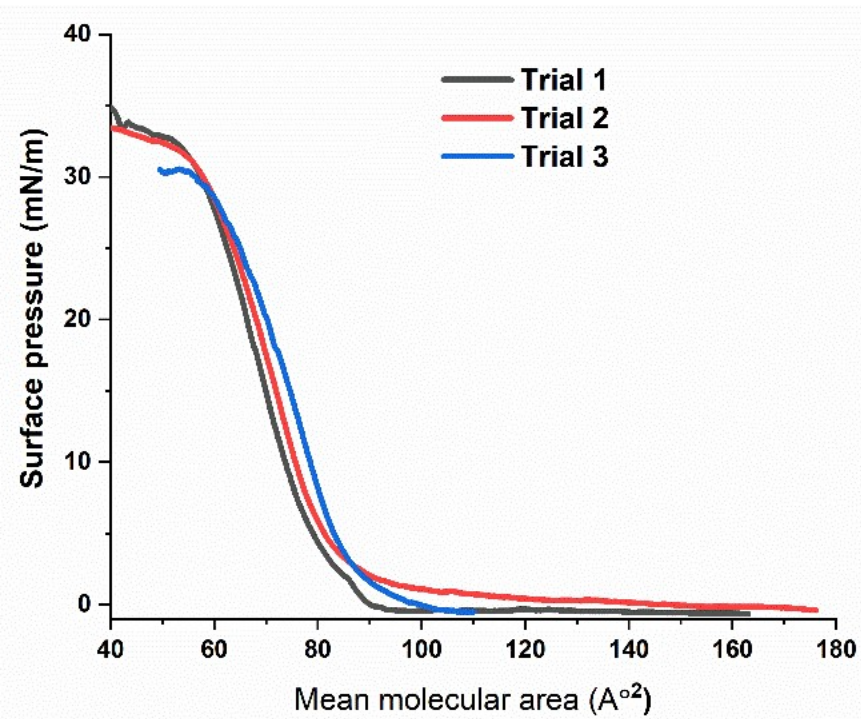
Figure S10. Isothermal compression data of complexes 1-4 (a-d)



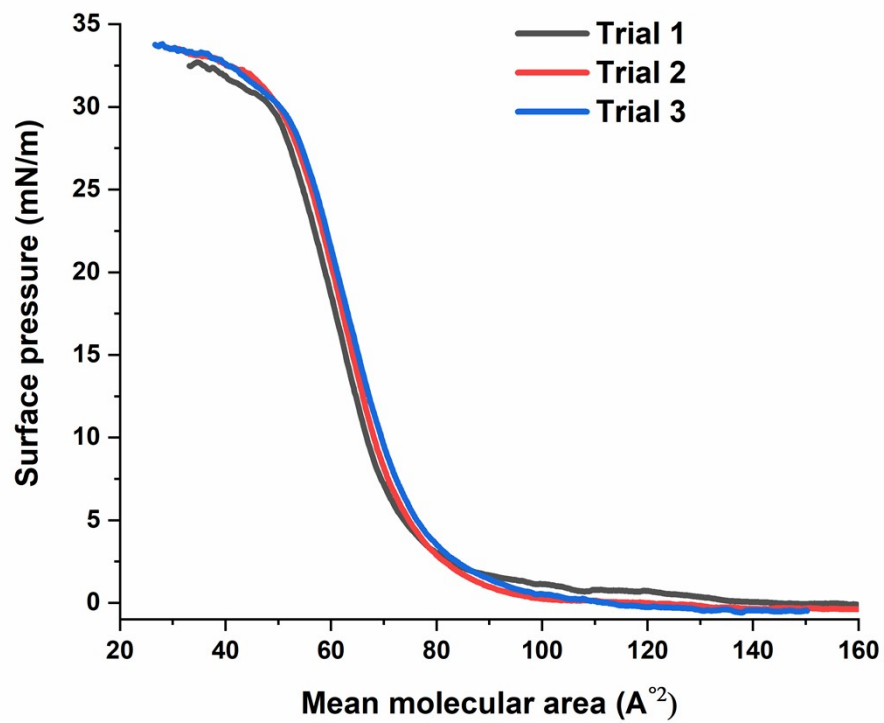
(a) Complex 1



(b) Complex 2



(c) Complex 3



(d) Complex 4

Figure S11: BAM Images of Complexes 1, 2 and 3

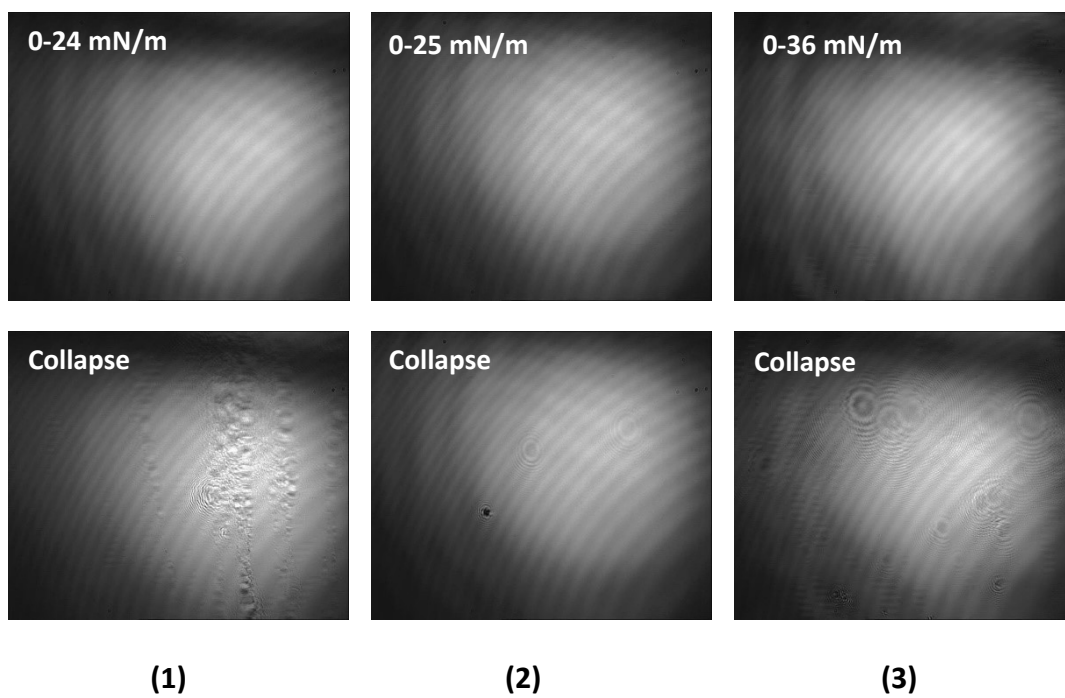


Table T3. Transfer ratios of monolayers of complexes 1-4

Complex	Transfer ratio 1	Transfer ratio 2	Transfer ratio 3
1	1.746	1.777	1.929
2	0.607	0.678	0.767
3	1.066	1.076	1.072
4	1.049	1.035	1.031

Figure S12. Comparison of UV-vis spectrum of LB films and solution state UV-vis spectrum of 3

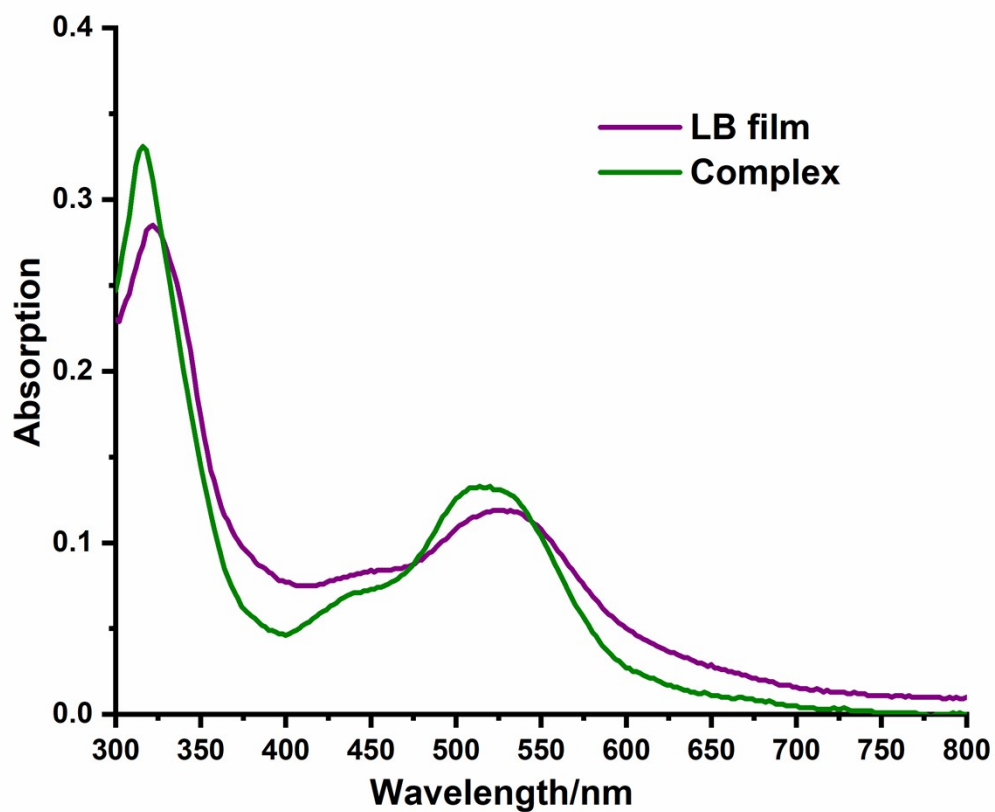


Figure S13: Comparison of UV-vis spectrum of LB films and solution state UV-vis spectrum of **4**

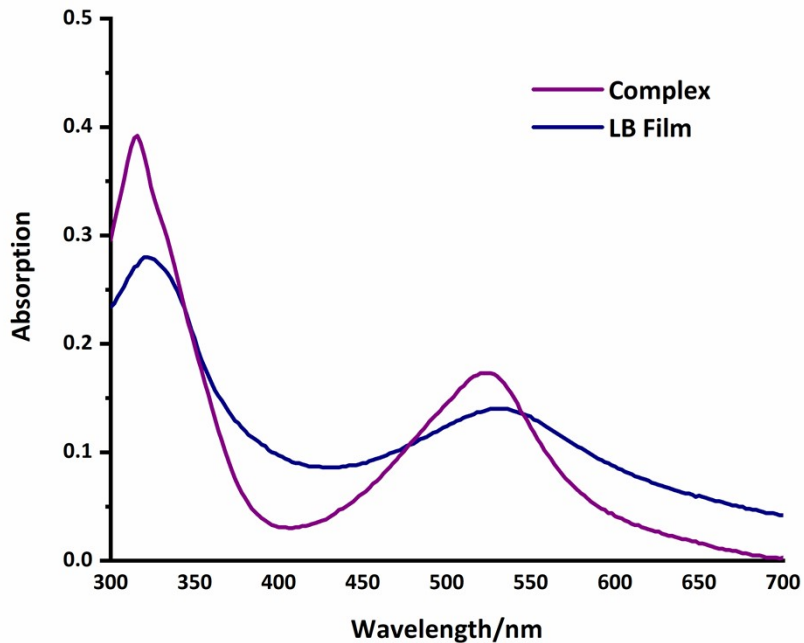


Figure S14: Comparison between IR spectrum of complex **4** in KBr and IRRAS spectrum of 47-layer LB film.

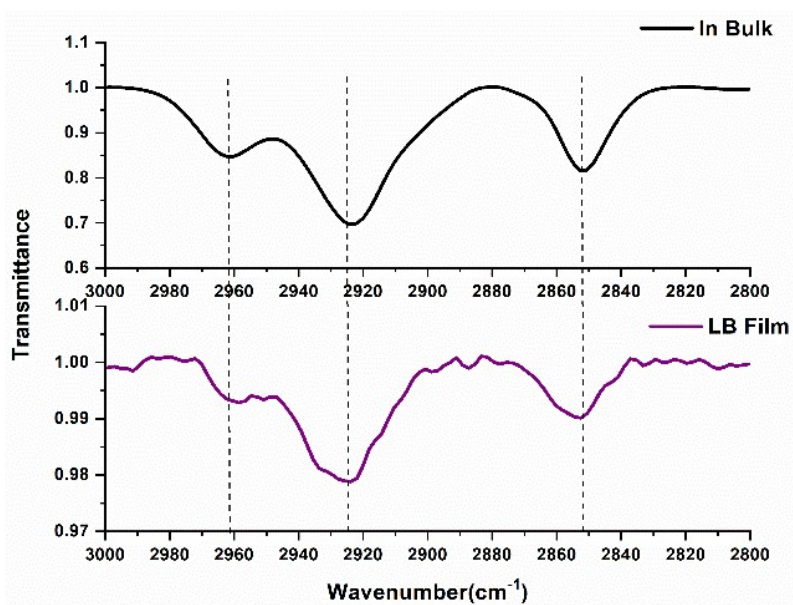
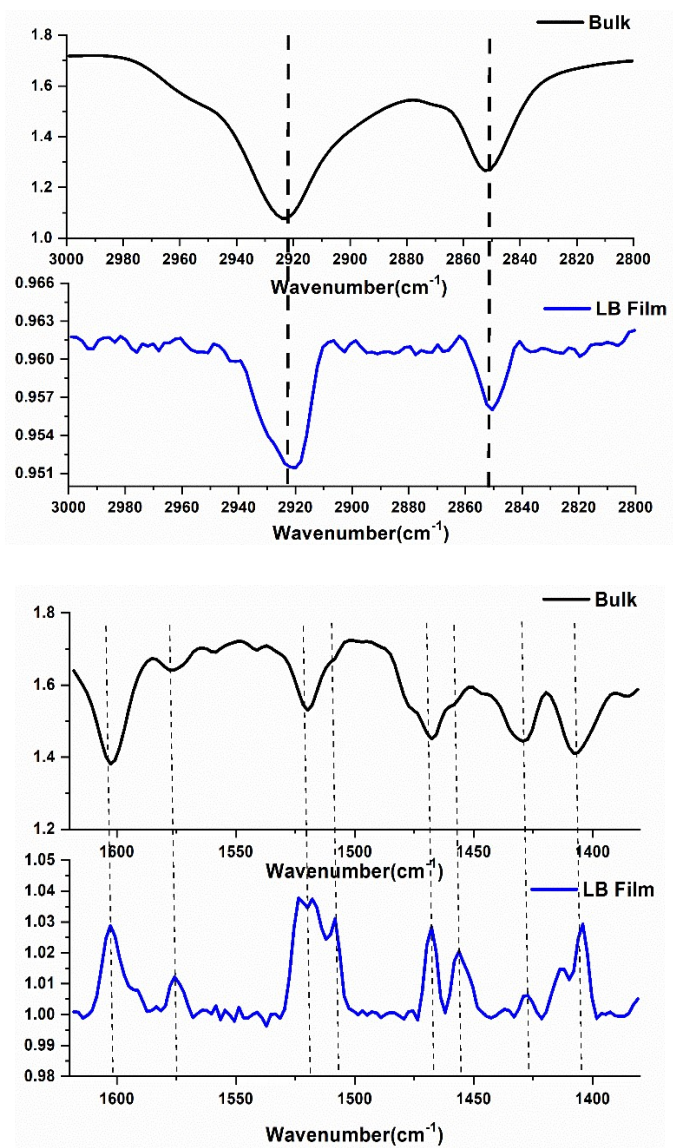


Figure S15: Comparison between IR spectrum of complex **3** in KBr and IRRAS spectrum of 47-layer LB film.



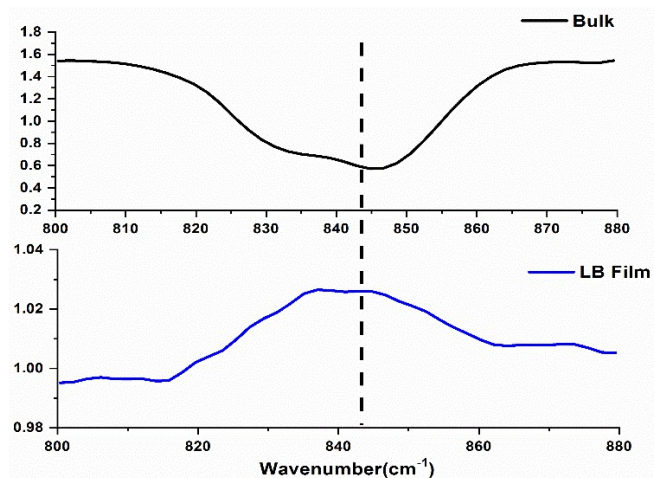


Figure S16: Mass spectrum of $[\text{Ru}(\text{tpy}^{\text{OC18}})(\text{phen})\text{Cl}](\text{PF}_6)$ **3** recovered from LB films

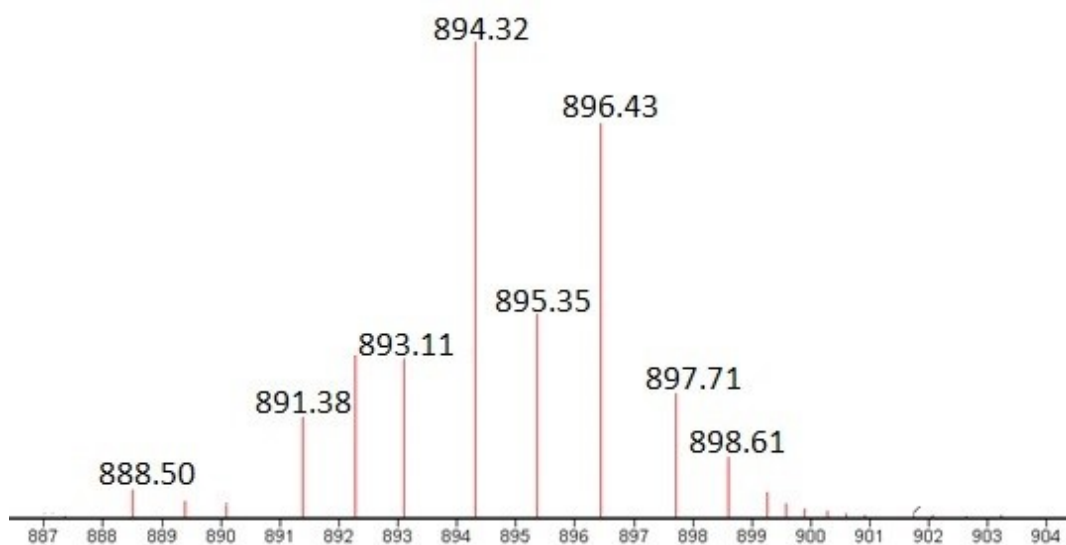


Figure S17: Mass spectrum of $[\text{Ru}(\text{tpy}^{\text{OC18}})(\text{phen}^{\text{NO2}})\text{Cl}](\text{PF}_6)$ **4** recovered from LB films

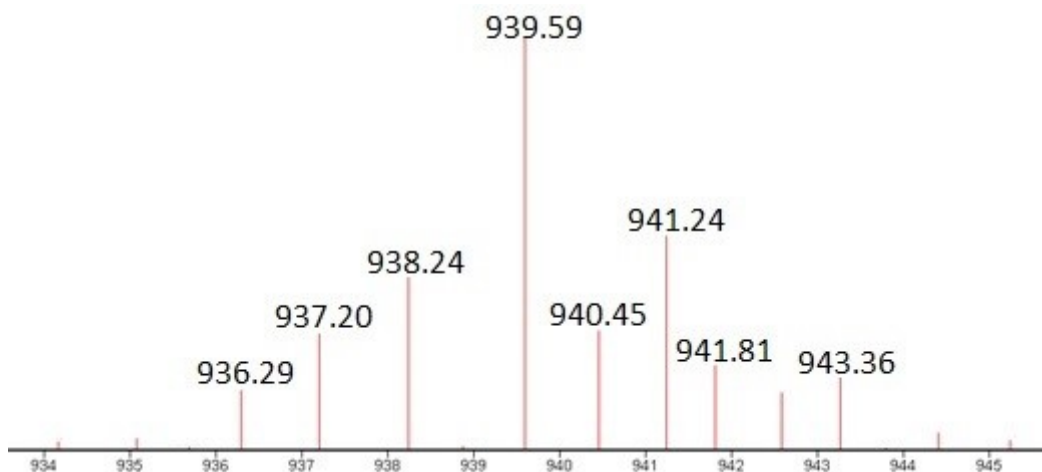


Figure S18: AFM images of complex **4** deposited at 18, 23, 27, and 30 mN/m

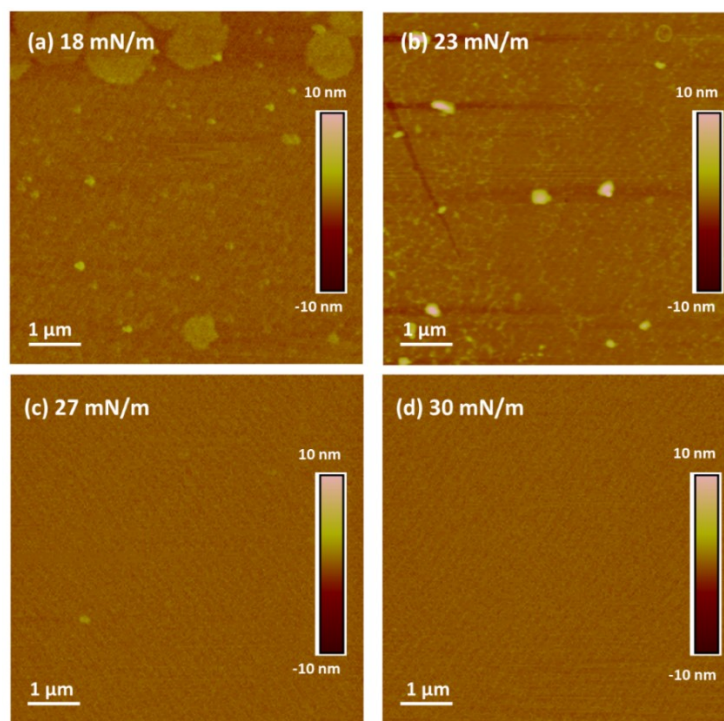


Table T4: Summary of surface roughness data of LB monolayers of complex **3** and **4** deposited at

Complex 3		Complex 4	
Pressure/mN/m	Roughness/nm	Pressure/mN/m	Roughness/nm
18	0.36 ± 0.1	17	0.22± 0.2
23	0.35 ± 0.5	20	0.12± 0.1
27	0.26 ± 0.5	24	0.31± 0.5
30	0.26 ± 0.1	28	0.32± 0.5

different pressures.

Figure S19: Asymmetric ruthenium(II) complexes investigated in the theoretical section (the -C₁₈H₃₇ group was replaced by a -CH₃ group)

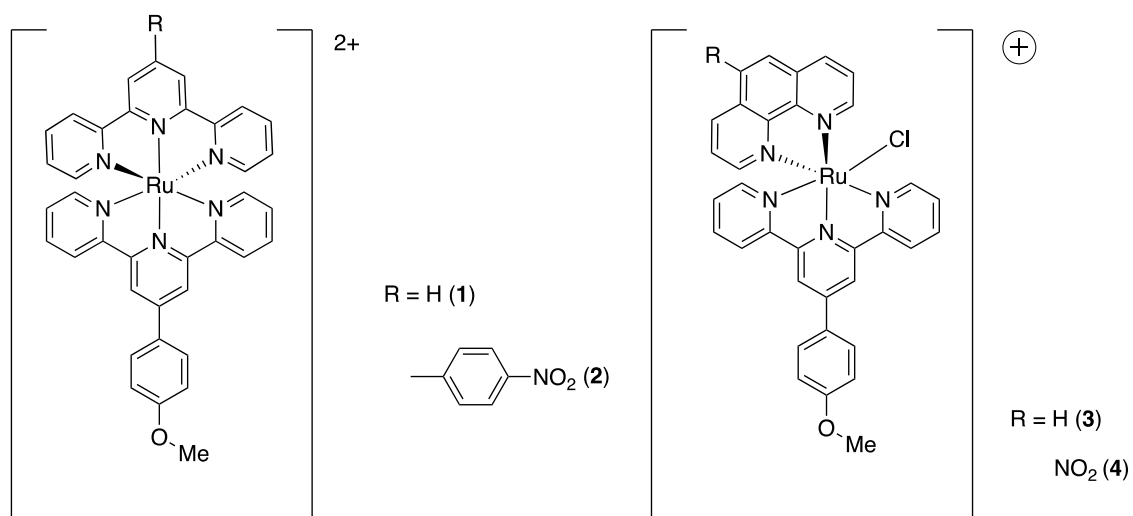


Figure S20: (a) Fragment orbital analysis of the singlet state of **1-3** (a-c) in dichloromethane

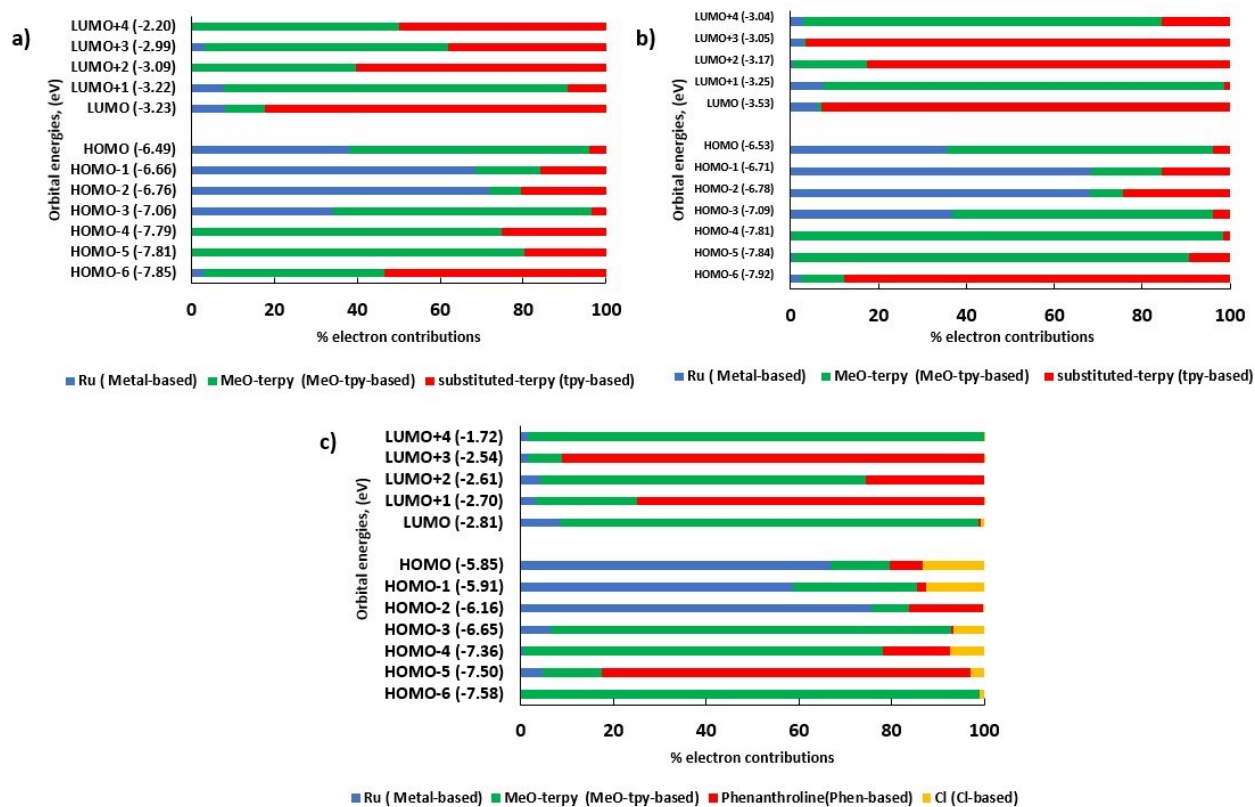


Figure S21: Ground state (singlet) frontier molecular orbitals of **1-3** complexes

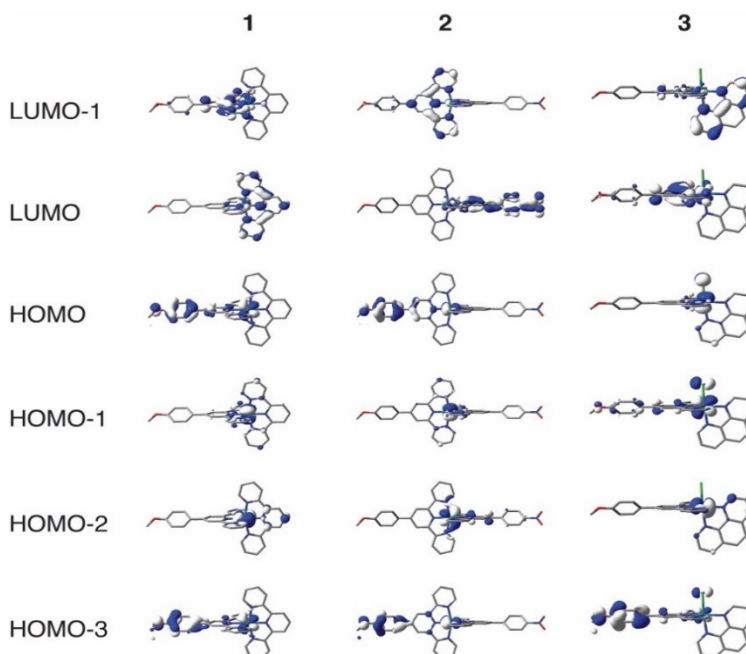


Figure S22: Molecular orbital diagram of asymmetric Ru complexes in their singlet ground state. MO colors correspond to their character; blue - metal-based, green - MeO-terpyridine-based,

purple - mixed character with contributions from Ru metal and MeO-terpyridine, brown - substituted terpyridine based, black – mixed character with contributions from MeO-terpyridine and substituted terpyridine, red - phenanthroline based)

The fragment schemes of the complexes:

1 and 2: Fragment 1: Ru
 Fragment 2: MeO-terpyridine
 Fragment 3: substituted terpyridine

3 and 4: Fragment 1: Ru
 Fragment 2: MeO-terpyridine
 Fragment 3: substituted phenanthroline
 Fragment 4: Cl

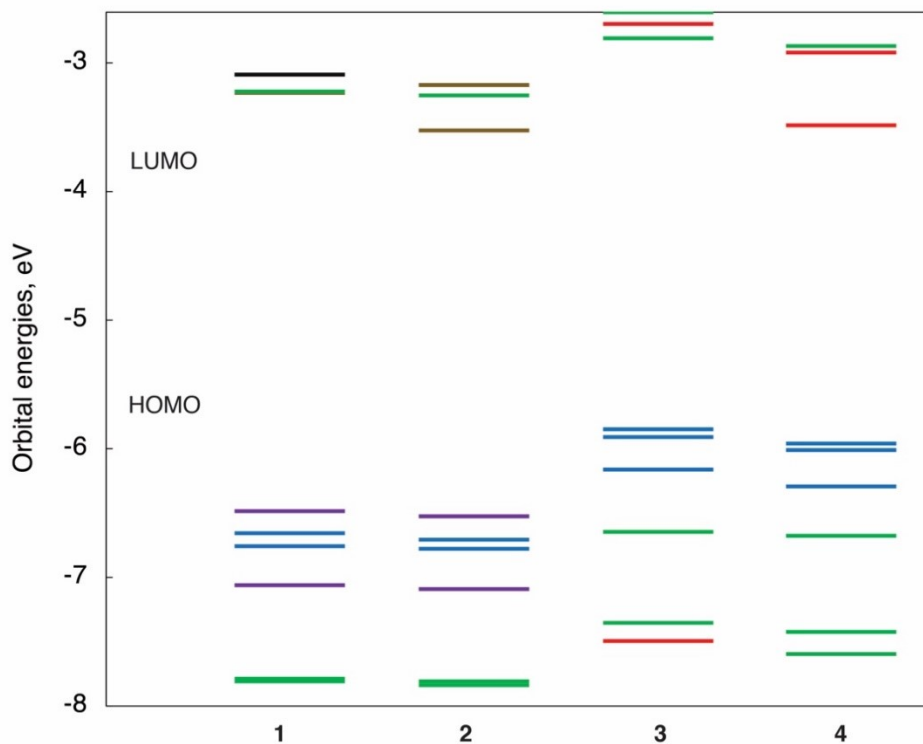
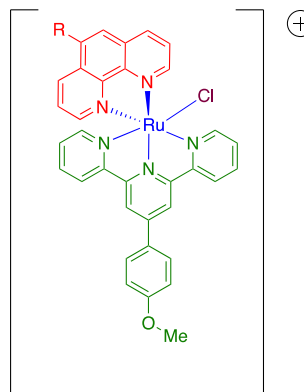
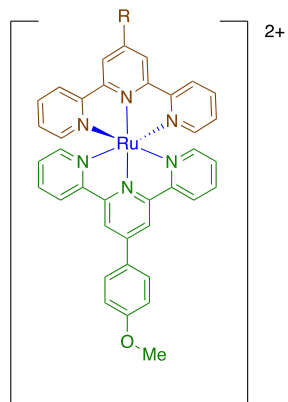


Figure S23: Natural orbitals (for open shell species) and molecular orbitals (for closed shell species) of the oxidized and reduced species of an asymmetric Ru complex **1** in dichloromethane. Orbital occupancy is shown for each orbital (0.0 – unoccupied orbital, 1.0 – singly-occupied orbital, 2.0 – doubly-occupied orbital).

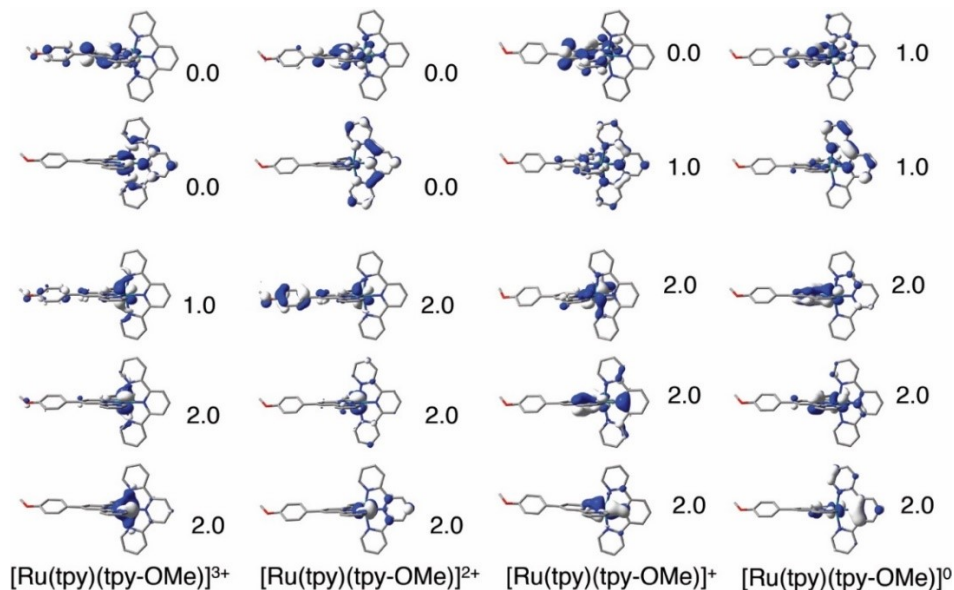


Figure S24: Natural orbitals (for open shell species) and molecular orbitals (for closed shell species) of the oxidized and reduced species of an asymmetric Ru complex **2** in dichloromethane. Orbital occupancy is shown for each orbital (0.0 – unoccupied orbital, 1.0 – singly-occupied orbital, 2.0 – doubly-occupied orbital).

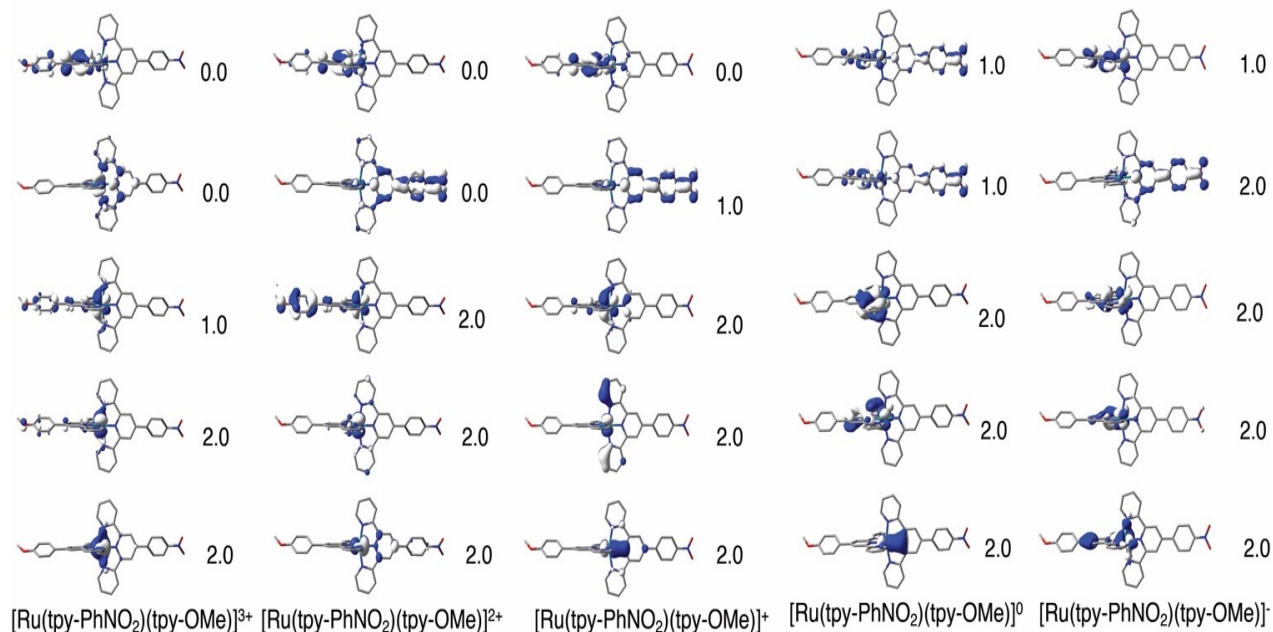


Figure S25: Natural orbitals (for open shell species) and molecular orbitals (for closed shell species) of the oxidized and reduced species of an asymmetric Ru complex **3** in dichloromethane. Orbital occupancy is shown for each orbital (0.0 – unoccupied orbital, 1.0 – singly-occupied orbital, 2.0 – doubly-occupied orbital).

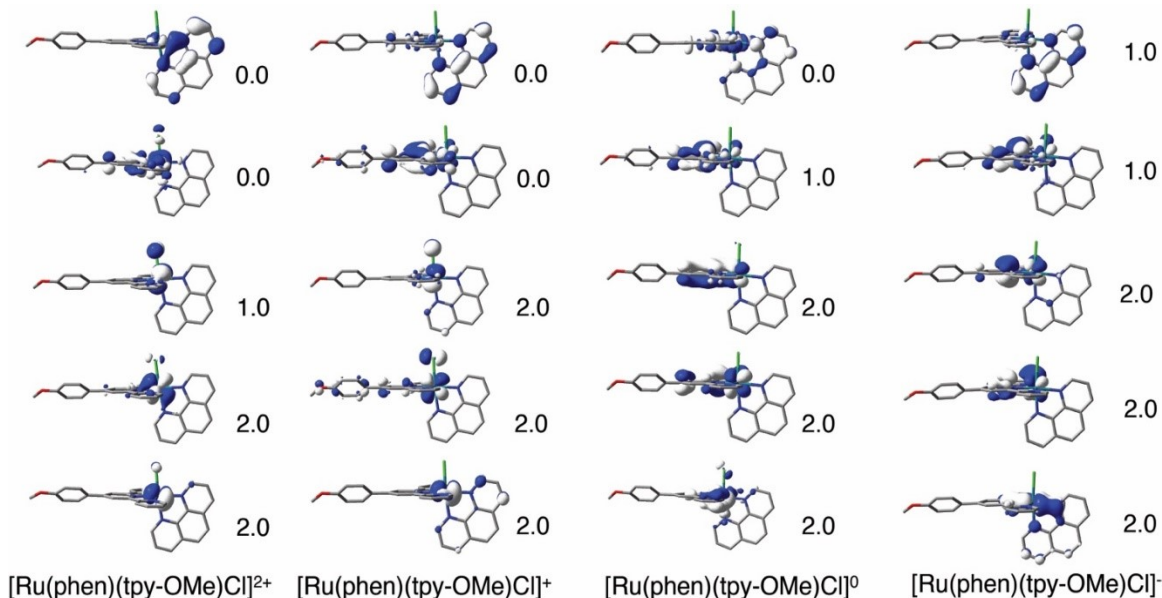


Figure S26: Natural orbitals (for open shell species) and molecular orbitals (for closed shell species) of the oxidized and reduced species of an asymmetric Ru complex **4** in dichloromethane. Orbital occupancy is shown for each orbital (0.0 – unoccupied orbital, 1.0 – singly-occupied orbital, 2.0 – doubly-occupied orbital).

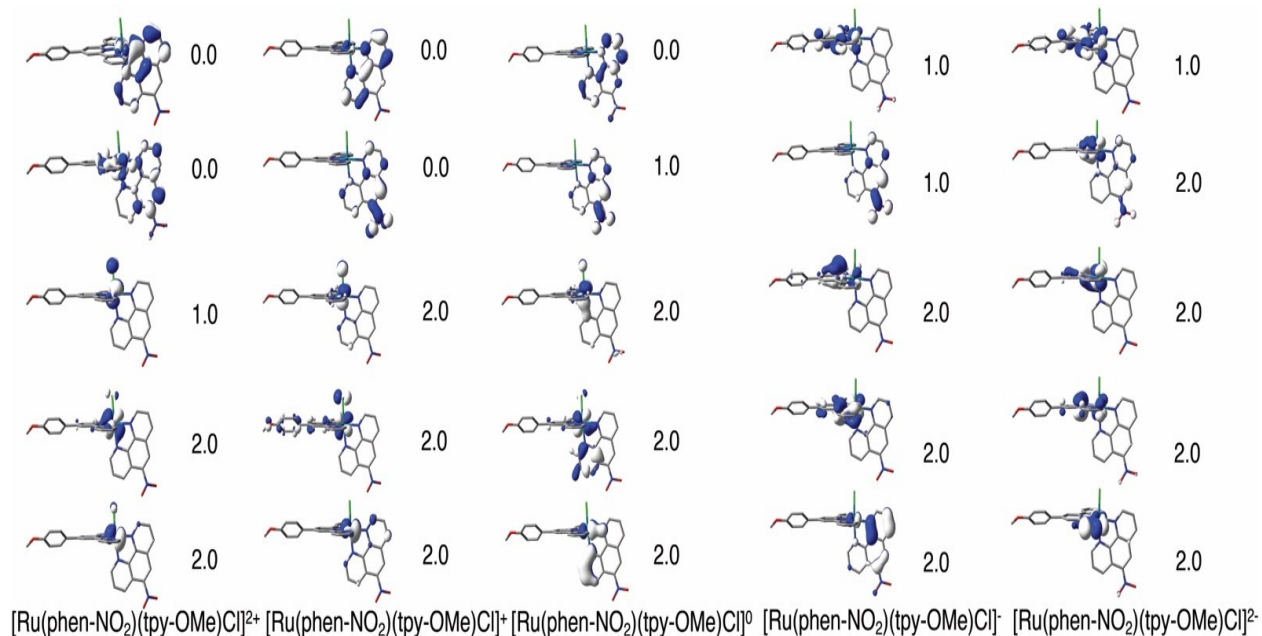
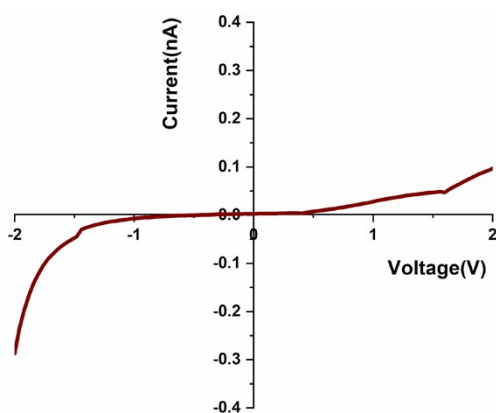
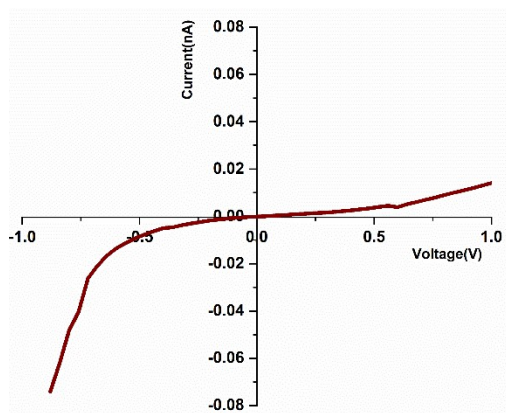
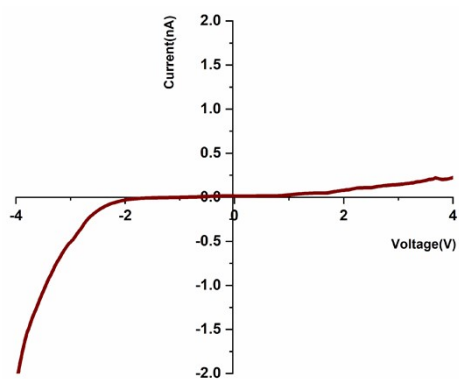
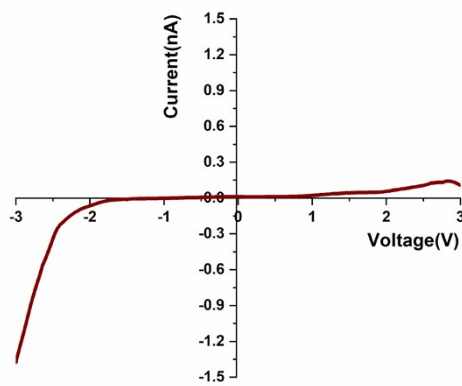
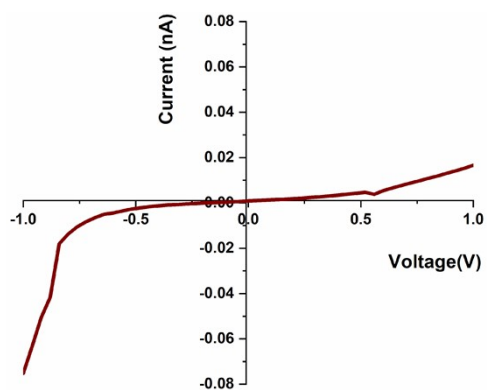


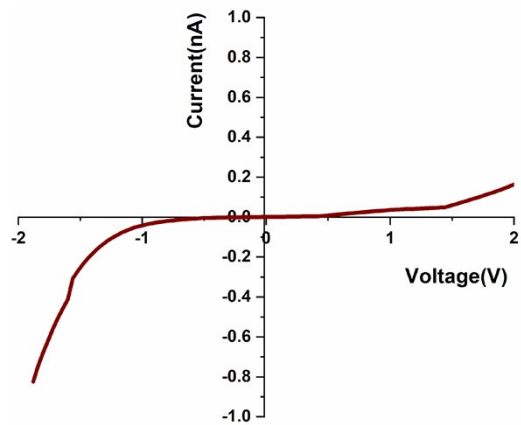
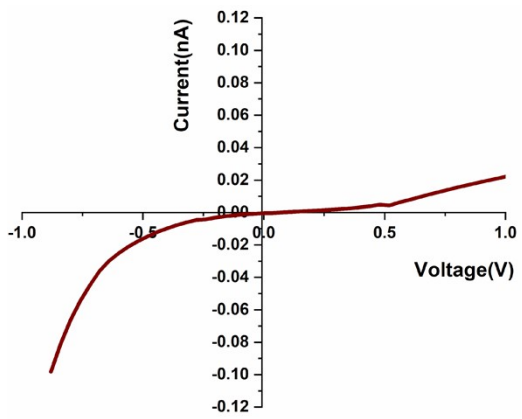
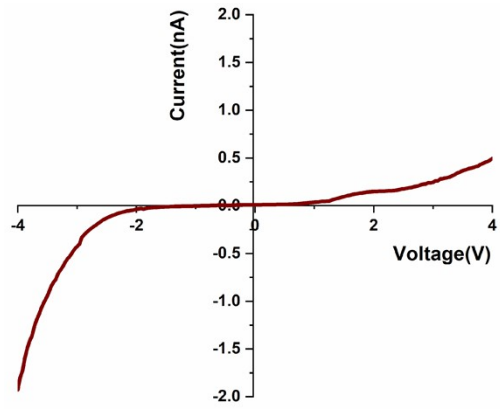
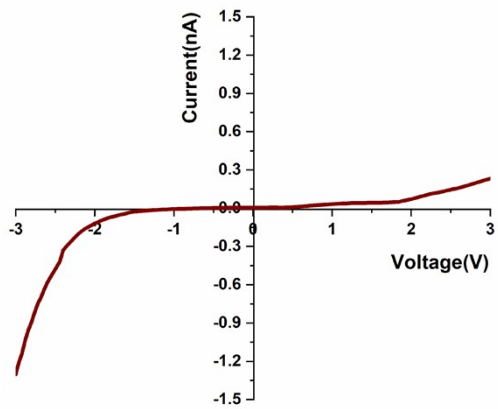
Table T5: Electrochemical data for asymmetric Ru(II) complexes in dichloromethane (PCM solvent model), S = singlet, D = doublet and T = triplet

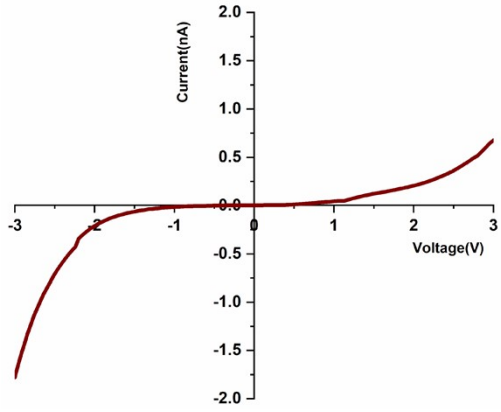
Redox reaction	$E_{1/2}$ (Calc.)	$E_{1/2}$ (Exp)	Assignment
$[\text{Ru}(\text{tpy})(\text{tpy-OMe})]^{3+} (\text{D}) \rightarrow [\text{Ru}(\text{tpy})(\text{tpy-OMe})]^{2+} (\text{S})$	1.28	0.87	Ru(II/III)
$[\text{Ru}(\text{tpy})(\text{tpy-OMe})]^{2+} (\text{S}) \rightarrow [\text{Ru}(\text{tpy})(\text{tpy-OMe})]^+ (\text{D})$	-1.33	-1.66	tpy/tpy ⁻
$[\text{Ru}(\text{tpy})(\text{tpy-OMe})]^+ (\text{D}) \rightarrow [\text{Ru}(\text{tpy})(\text{tpy-OMe})]^0 (\text{T})$	-2.12	-1.98	tpy/tpy ⁻
$[\text{Ru}(\text{NO}_2\text{-tpy})(\text{tpy-OMe})]^{3+} (\text{D}) \rightarrow [\text{Ru}(\text{NO}_2\text{-tpy})(\text{tpy-OMe})]^{2+} (\text{S})$	1.34	0.88	Ru(II/III)
$[\text{Ru}(\text{NO}_2\text{-tpy})(\text{tpy-OMe})]^{2+} (\text{S}) \rightarrow [\text{Ru}(\text{NO}_2\text{-tpy})(\text{tpy-OMe})]^+ (\text{D})$	-1.16	-1.34	NO ₂ /NO ₂ ⁻
$[\text{Ru}(\text{NO}_2\text{-tpy})(\text{tpy-OMe})]^+ (\text{D}) \rightarrow [\text{Ru}(\text{NO}_2\text{-tpy})(\text{tpy-OMe})]^0 (\text{T})$	-1.81	-1.56	tpy/tpy ⁻
$[\text{Ru}(\text{NO}_2\text{-tpy})(\text{tpy-OMe})]^0 (\text{T}) \rightarrow [\text{Ru}(\text{NO}_2\text{-tpy})(\text{tpy-OMe})]^- (\text{D})$	-2.46	-1.94	tpy/tpy ⁻
$[\text{Ru}(\text{phen})(\text{tpy-OMe})\text{Cl}]^{2+} (\text{D}) \rightarrow [\text{Ru}(\text{phen})(\text{tpy-OMe})\text{Cl}]^+ (\text{S})$	0.50	0.35	Ru(II/III)
$[\text{Ru}(\text{phen})(\text{tpy-OMe})\text{Cl}]^+ (\text{S}) \rightarrow [\text{Ru}(\text{phen})(\text{tpy-OMe})\text{Cl}]^0 (\text{D})$	-1.86	-1.91	tpy/tpy ⁻
$[\text{Ru}(\text{phen})(\text{tpy-OMe})\text{Cl}]^0 (\text{D}) \rightarrow [\text{Ru}(\text{phen})(\text{tpy-OMe})\text{Cl}]^- (\text{T})$	-2.49	-2.40	phen/phen ⁻
$[\text{Ru}(\text{NO}_2\text{-phen})(\text{tpy-OMe})\text{Cl}]^{2+} (\text{D}) \rightarrow [\text{Ru}(\text{NO}_2\text{-phen})(\text{tpy-OMe})\text{Cl}]^+ (\text{S})$	0.58	0.48	Ru(II/III)
$[\text{Ru}(\text{NO}_2\text{-phen})(\text{tpy-OMe})\text{Cl}]^+ (\text{S}) \rightarrow [\text{Ru}(\text{NO}_2\text{-phen})(\text{tpy-OMe})\text{Cl}]^0 (\text{D})$	-1.15	-1.06	NO ₂ /NO ₂ ⁻
$[\text{Ru}(\text{NO}_2\text{-phen})(\text{tpy-OMe})\text{Cl}]^0 (\text{D}) \rightarrow [\text{Ru}(\text{NO}_2\text{-phen})(\text{tpy-OMe})\text{Cl}]^{1-} (\text{T})$	-2.15	-1.71	tpy/tpy ⁻
$[\text{Ru}(\text{NO}_2\text{-phen})(\text{tpy-OMe})\text{Cl}]^{1-} (\text{T}) \rightarrow [\text{Ru}(\text{NO}_2\text{-phen})(\text{tpy-OMe})\text{Cl}]^{2-} (\text{D})$	-2.90	-2.08	phen/phen ⁻

Figure S27: I-V characteristics of complex 4 in four devices

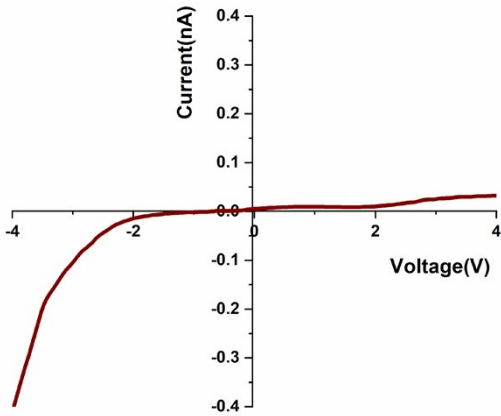
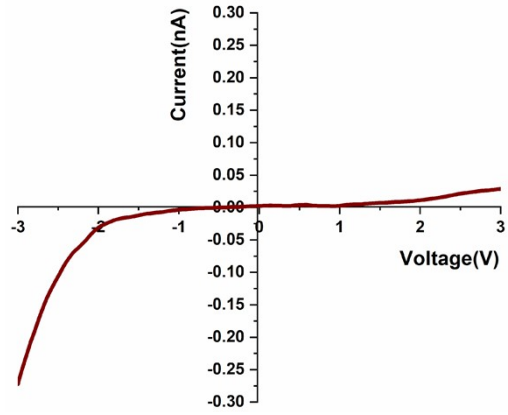
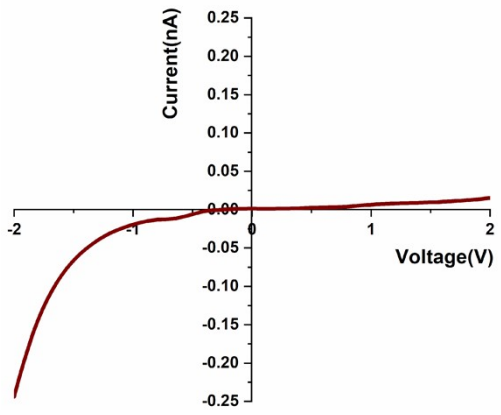
Assembly 1



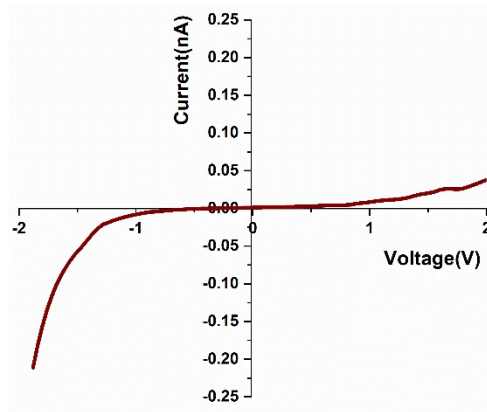
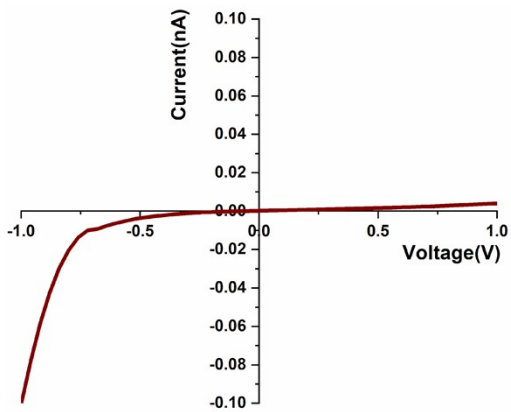
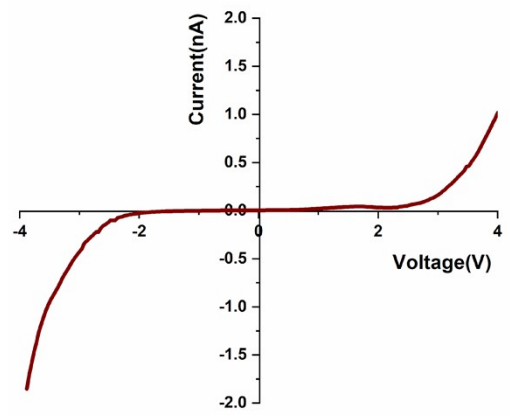
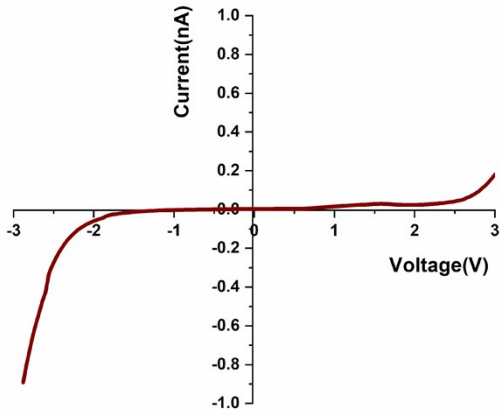
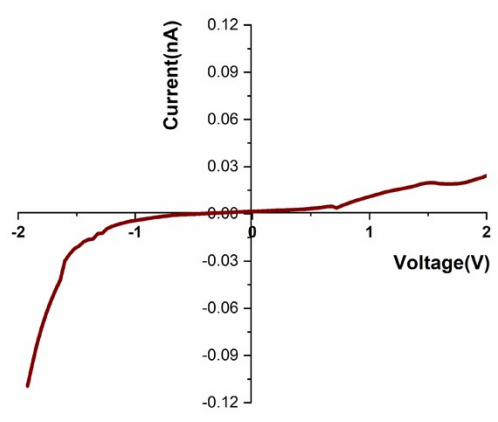
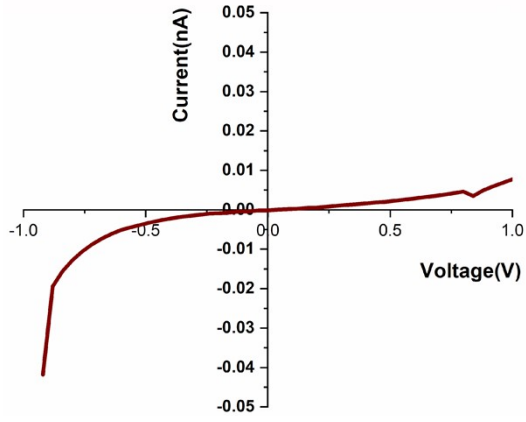




Assembly 2



Assembly 3



Assembly 3

